JOURNAL OF SPACECRAFT AND ROCKETS
Vol. 36, No. 2, March–April 1999

# Ceramics Catalysis Evaluation at High Temperature Using Thermal and Chemical Approaches

M. J. H. Balat,* M. Czerniak,† and J. M. Badie‡
*Centre National de la Recherche Scientifique, 66125 Font-Romeu Odeillo, France*

**During the atmospheric re-entry phase, the physicochemical phenomena taking place on space vehicle walls can lead to an important excess of heating and damage of the protective materials. The catalytic recombination of atomic oxygen under conditions nearby Earth's atmospheric re-entry is studied. The most important conditions for the simulation (high-temperature, low-pressure air plasma) have been realized in the MESOX setup, which associates a solar radiation concentrator and a microwave generator. Concerning the dynamic contribution, only low-enthalpy flow is reproduced. Study of atomic oxygen recombination on partially catalytic silicon- or aluminum-based ceramic materials at high temperature (1000–1800 K) is done at different pressures (200–2000 Pa) by a thermal approach (macroscopic) and leads to a catalytic scale of materials. The influence of the pressure on the studied range is very weak, but the surface temperature strongly changes the catalytic activity of these materials. The variations are weak in the case of sintered SiC, for which the catalytic recombination flux is about 32 $kW \cdot m^{-2}$, but are more important in the case of sintered $Al_2O_3$, being more catalytic, with fluxes between 65 and 185 $kW \cdot m^{-2}$ on the whole pressure range. Alternatively, a chemical approach (microscopic) is developed for the evaluation of the catalytic recombination coefficient $\gamma$ using emission spectroscopy (actinometry) on the same device. The partial catalytic scale obtained by this method is well suited to that of the thermal approach.**

## Nomenclature

$A$ = atom
$C$ = concentration, atom/$m^3$
$D$ = binary diffusion coefficient, $cm^2/s$
$I$ = intensity, AU
$k_B$ = Boltzmann constant
$L$ = thickness of the boundary layer, m
$M$ = molar mass, g/mol
$N_A$ = Avogadro number
$P$ = total pressure, Pa
$q$ = thermal flux, $W/m^2$
$R$ = ratio of intensity $I$
$r$ = radius, m
$T$ = temperature, K
$t$ = time, s
$U$ = mass transfer velocity, m/s
$V$ = mean square atomic velocity, m/s
$x$ = abscissa, m
$\alpha$ = solar absorptivity coefficient
$\beta$ = accommodation coefficient
$\gamma$ = recombination coefficient
$\Delta T$ = difference between two temperatures, K
$\varepsilon$ = total hemispherical emissivity
$\lambda$ = wavelength, $\mu$m
$\sigma$ = Stefan–Boltzmann constant
$\omega$ = variation of concentration

*Subscripts*

$A$ = atom
Ar = argon
$b$ = back face of the sample
conv = convective transfer
$f$ = front face of the sample
$g$ = gas
$L$ = distance from the sample surface
lat = lateral thermal losses at the limit of the reference cylinder
mw = microwave (microwave–material interaction)
O = atomic oxygen
rad = radiative transfer
rec = recombination
sol = solar
0 = zero, where $x$ is 0

*Superscripts*

air = under airflow
arg = under argon flow
$*$ = under plasma conditions

## Introduction

THE development of thermal protection materials for space vehicles needs surface flux calculations during atmospheric re-entry to predict heat rates. Most of the experiments were realized in arc-plasma test facilities, where the recombination is obtained from stagnation point heat flux measurement in dissociated arc jet flow. The relative heating rates of a known catalytic sample are compared to the surface being studied.[1–10]

Some evaluation of catalytic recombination is obtained by measurement of atom concentration by several techniques (laser-induced fluorescence, spectroscopy, etc.)[11–13] to reach the recombination coefficient $\gamma$. Other authors have proposed models for recombination and compared them to experimental values.[2,4,14,15]

Another coefficient, $\beta$, accommodation, is rarely evaluated, and often its value is taken equal to 1. Some authors have tried to measure $\beta$, and the result is often far from 1 (Refs. 16–20). This coefficient is very important because it allows taking into account the real energy transferred to the surface.

Often, measurements of both flux and of the $\gamma$ coefficient to study the recombination process are not realized in the same experiment. More often, the flux is measured, and the recombination coefficient $\gamma$ is obtained by calculation. The experimental setup that we have developed in our laboratory allows the simultaneous measurement of the thermal and chemical contributions of the atomic oxygen recombination on the surface on the same setup, and so the accuracy may be better.

Presented as Paper 97-2589 at the AIAA 32nd Thermophysics Conference, Atlanta, GA, June 23–25, 1997; received July 30, 1997; revision received April 28, 1998; accepted for publication Nov. 9, 1998. 

*Senior Scientist, Institut de Science et de Génie des Matériaux et Procédés, Unité Propre 8521, BP 5. Member AIAA.
†Ph.D. Student, Institut de Science et de Génie des Matériaux et Procédés, Unité Propre 8521, BP 5.
‡Senior Scientist, Institut de Science et de Génie des Matériaux et Procédés, Unité Propre 8521, BP 5.

## Experimental Setup

The MESOX setup, which associates a solar radiation concentrator for the sample heating (up to 2300 K under pressures between $10^2$ and $10^5$ Pa) and a microwave generator, originally developed for oxidation studies,[21] has been adapted to allow catalytic recombination measurements. Atmospheric re-entry conditions can be partially simulated[22,23] (air plasma with $O_2$ partially dissociated, no dissociation of $N_2$ or NO present, verified by emission spectroscopy), and pressure and temperature can be reproduced independently with high accuracy in contrast to various types of wind tunnels.

The experimental device (Fig. 1) is placed at the focus of a solar furnace equipped with a shutter with variable opening and can be moved away from the focus to be replaced by a calorimeter to measure the incident solar flux. The available incident concentrated solar flux can reach 4.5 MW/m$^2$. The temperature measurements on the front and back faces of the sample, $T_f$ and $T_b$, respectively, are realized using a single optical pyrometer ($\lambda$ centred at 5 $\mu$m) with one rotating mirror and a system of two stationary mirrors.

The experimental chamber consists of a silica tube 50 cm in length and 5 cm in diameter with $CaF_2$ viewports at the extremities for pyrometry measurements. This reactor crossing the refrigerated waveguide contains the sample (25-mm diam and 3-mm height) placed on a zirconia sample holder in the stagnation point position at the center of the discharge.

The microwave generator works at power between 0 and 1200 W at a frequency of 2450 MHz. The working power used in this study is 300 W. A regulator, a gauge, and a vacuum pump are used to control precisely the total pressure during the experiment.

## Thermal Approach: Heat Balance

We have developed a thermal approach for atomic oxygen recombination evaluation using a heat balance on a reference cylinder volume in the sample. The surface of this cylinder of 6-mm diam and 3-mm height in the sample, considered for the thermal balance (Fig. 2), represents the measurement area by pyrometry. Convective phenomena are neglected (rarefied gas flows), compared to the radiative fluxes, to establish the equations for steady-state heat transfer under different environments. The thermal balance is established under each atmosphere: standard air, air plasma, standard argon, and argon plasma, the recombination flux being determined by the difference between the experiments under air plasma (reactive) and under argon plasma (inert).

Under standard air, the sample is heated only by solar radiation:

$$\alpha \cdot q_{\mathrm{sol}}^{\mathrm{air}} = q_{\mathrm{rad},f}^{\mathrm{air}} + q_{\mathrm{rad},b}^{\mathrm{air}} + q_{\mathrm{lat}}^{\mathrm{air}} \tag{1}$$

Under air plasma, the sample is heated by solar radiation, by microwave–material interaction, and by atomic oxygen recombination:

$$\alpha \cdot q_{\mathrm{sol}}^{\mathrm{air},*} + q_{\mathrm{mw}}^{\mathrm{air},*} + \beta \cdot q_{\mathrm{rec}}^{\mathrm{air},*} = q_{\mathrm{rad},f}^{\mathrm{air},*} + q_{\mathrm{rad},b}^{\mathrm{air},*} + q_{\mathrm{lat}}^{\mathrm{air},*} \tag{2}$$

Under standard argon, the sample is heated only by solar radiation as with standard air:

$$\alpha \cdot q_{\mathrm{sol}}^{\mathrm{arg}} = q_{\mathrm{rad},f}^{\mathrm{arg}} + q_{\mathrm{rad},b}^{\mathrm{arg}} + q_{\mathrm{lat}}^{\mathrm{arg}} \tag{3}$$

Under argon plasma, the sample is heated by solar radiation and by microwave–material interaction:

$$\alpha \cdot q_{\mathrm{sol}}^{\mathrm{arg},*} + q_{\mathrm{mw}}^{\mathrm{arg},*} = q_{\mathrm{rad},f}^{\mathrm{arg},*} + q_{\mathrm{rad},b}^{\mathrm{arg},*} + q_{\mathrm{lat}}^{\mathrm{arg},*} \tag{4}$$

The recombination flux is obtained by the difference between Eqs. (2) and (4), and we can neglect the difference between the radial losses by conduction out of the reference cylinder because the radial losses are of the same order in air and in argon plasmas. Under the following assumptions (some are experimentaly verified) a quasi-one-dimensional equation is obtained:

1) Without plasma, the same temperature level is reached for both air and argon atmospheres, that is, $T_f^{\mathrm{air}} = T_f^{\mathrm{arg}}$ and $T_b^{\mathrm{air}} = T_b^{\mathrm{arg}}$; this is due to the constant solar flux, the experiments being done around the period of solar zenith.

2) Under plasma, the microwave–material interaction for both the atmospheres is supposedly equal, and so $q_{\mathrm{mw}}^{\mathrm{air},*} = q_{\mathrm{mw}}^{\mathrm{arg},*}$; this will be verified when the dielectric permittivity of the samples tested is measured at high temperature, and so the absorbed power will be known.

3) The absorbed solar energy is constant under different atmospheres for a given shutter opening because during all of the experiment the incident solar flux is constant.

4) The radial losses by conduction out of the reference cylinder are neglected. Infrared imaging on the front face of the sample has permitted the determination of a weak radial temperature gradient as a function of distance from the center, even when the sample is heated under air or argon plasma.[23] Therefore, the thermal balance is reduced to a one-dimensional approach. Finally,

$$\beta \cdot q_{\mathrm{rec}}^{\mathrm{air},*} = q_{\mathrm{rad},f}^{\mathrm{air},*} - q_{\mathrm{rad},f}^{\mathrm{arg},*} + q_{\mathrm{rad},b}^{\mathrm{air},*} - q_{\mathrm{rad},b}^{\mathrm{arg},*} \tag{5}$$

equivalent to

$$\beta \cdot q_{\mathrm{rec}}^{\mathrm{air},*} = \varepsilon\sigma\left[\left(T_f^{\mathrm{air},*}\right)^4 - \left(T_f^{\mathrm{arg},*}\right)^4 + \left(T_b^{\mathrm{air},*}\right)^4 - \left(T_b^{\mathrm{arg},*}\right)^4\right] \tag{6}$$

The absorbed recombination flux can be calculated from the following parameters: the total hemispherical emissivity $\varepsilon$ and the front- and back-face temperatures under air and argon plasmas, $T_f^*$ and $T_b^*$.

The uncertainties $\Delta\beta \cdot q_{\mathrm{rec}}/\beta \cdot q_{\mathrm{rec}}$ have been calculated, taking into account the errors in temperature measurements due to the accuracy of the optical pyrometer (0.5%), in the spectral emissivity (at 5 $\mu$m, 1–2% depending on the materials) and in the total hemispherical emissivity (1%). The emissivity measurements are done in our laboratory by a direct method using a two-color (1.3- and 1.55-$\mu$m) pyrometer for the temperature measurement and a spectroradiometer for the luminance determination. The accuracy is given in Tables 1 and 2 but not in the figures for better visualization of the experimental points.

### Experimental Results

The pressure and the flow rate ($1.11 \times 10^{-6}$ m$^3 \cdot$ s$^{-1}$) were fixed at the beginning of each experiment. Three total gas pressures, 200, 1000, and 2000 Pa, were applied for five temperature levels (1000, 1200, 1400, 1600, and 1800 K). The surface temperature depends on the incident solar flux controlled by the opening of the shutter.

This study was realized on sintered materials (SiC, $Si_3N_4$, AlN, $Al_2O_3$) or on samples obtained by oxidation at 1300 K during 24 h ($SiC + SiO_2$, $AlN + Al_2O_3$).

Figure 3 shows the temperature increase due to the atomic oxygen recombination on the surface of different materials deduced from the difference under air and argon plasmas at 200 Pa:

$$\Delta T_f = T_f^{\mathrm{air},*} - T_f^{\mathrm{air}} - \left(T_f^{\mathrm{arg},*} - T_f^{\mathrm{arg}}\right) \tag{7}$$

**Table 1 Experimental data for atomic oxygen recombination on sintered SiC at 200-Pa total air pressure**

| $T_f$,[a] K | $\Delta T_f$[b] | $\beta \cdot q_{\mathrm{rec}}^{\mathrm{2D}}$,[c] kW/m$^2$ | $\beta \cdot q_{\mathrm{rec}}^{\mathrm{1D}}$,[c] kW/m$^2$ |
|---|---|---|---|
| 984 ± 3 | 64 | 35 | 30 ± 3 |
| 1191 ± 5 | 38 | 33 | 29 ± 2 |
| 1377± 7 | 27 | 33 | 30 ± 3 |
| 1591 ± 9 | 16 | 27 | 25 ± 2 |
| 1780 ± 11 | 7 | 13 | 13 ± 2 |

[a]Front-face temperature.
[b]Front-face temperature increase due to recombination.
[c]Two- and one-dimensional experimental flux transferred to the surface.

**Table 2 Experimental data for atomic oxygen recombination on sintered $Al_2O_3$ at 200-Pa total air pressure**

| $T_f$,[a] K | $\Delta T_f$[b] | $\beta \cdot q_{\mathrm{rec}}^{\mathrm{2D}}$,[c] kW/m$^2$ | $\beta \cdot q_{\mathrm{rec}}^{\mathrm{1D}}$,[c] kW/m$^2$ |
|---|---|---|---|
| 975 ± 6 | 281 | 110 | 97 ± 16 |
| 1168 ± 9 | 287 | 155 | 139 ± 24 |
| 1399 ± 12 | 251 | 161 | 151 ± 29 |
| 1577 ± 16 | 153 | 112 | 108 ± 23 |
| 1710 ± 20 | 81 | 66 | 65 ± 15 |

[a]Front-face temperature.
[b]Front-face temperature increase due to recombination.
[c]Two- and one-dimensional experimental flux transferred to the surface.

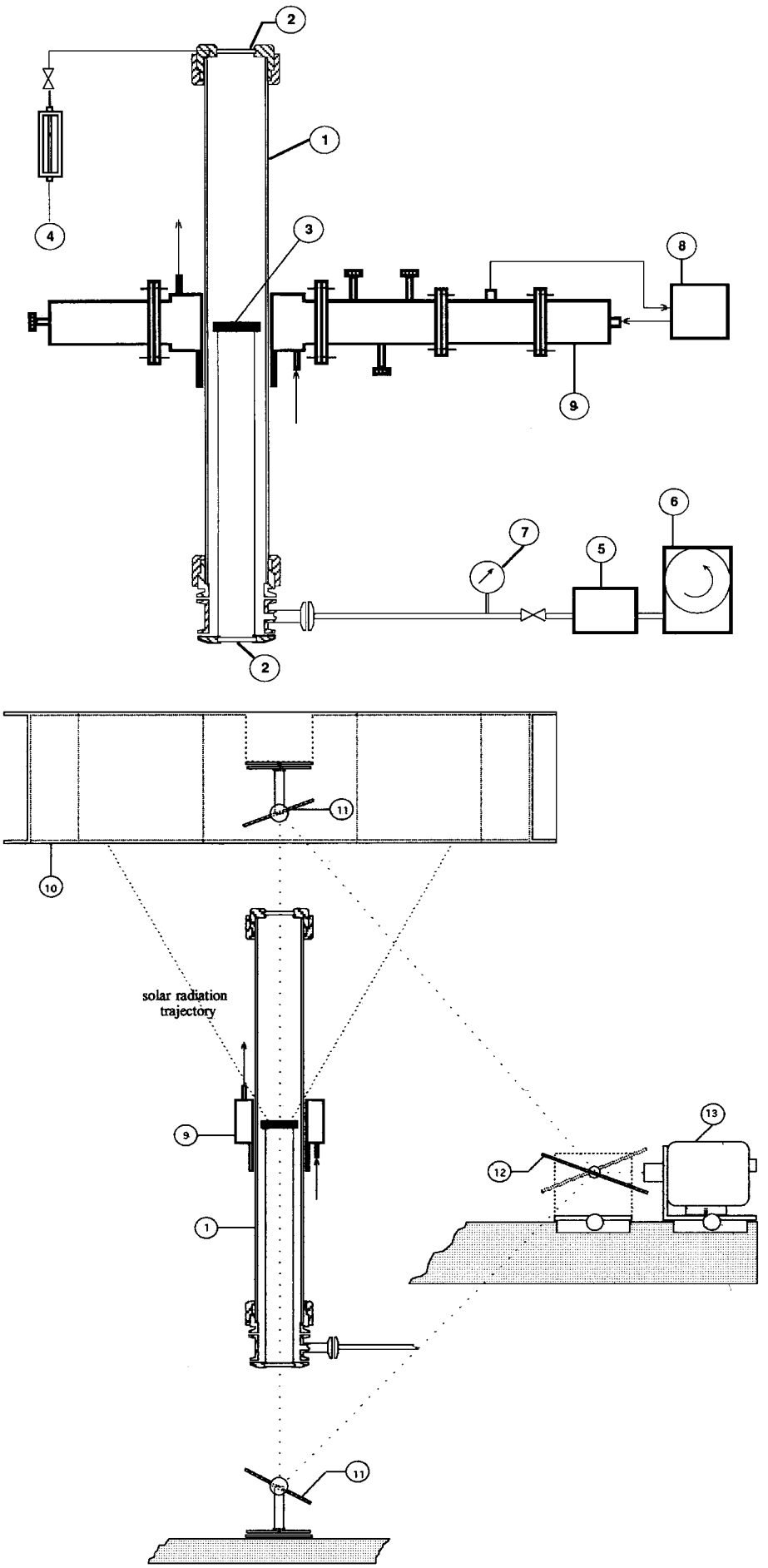


**Fig. 1 Experimental setup: 1) silica vessel, 2) viewports, 3) sample, 4) flowmeter, 5) pressure regulator, 6) vacuum pump, 7) pressure gauge, 8) microwave generator, 9) waveguide, 10) shutter, 11) fixed mirror, 12) rotating mirror, and 13) optical pyrometer.**

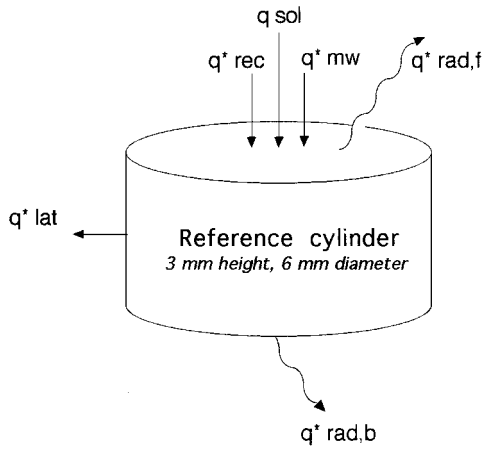


**Fig. 2 Heat flux representation on the reference cylinder (6-mm diam, 3-mm height) on the sample (25-mm diam, 3-mm height) heated by solar radiation under microwave air plasma conditions.**

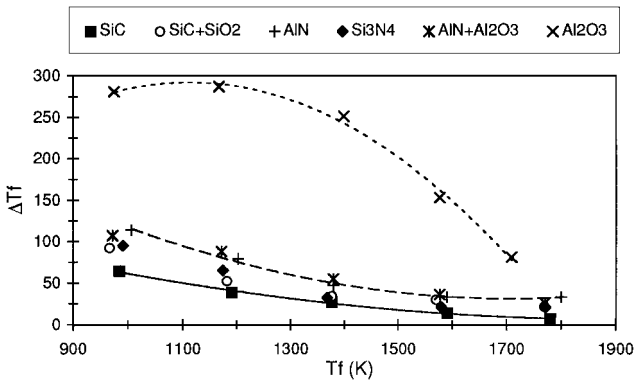


**Fig. 3 Temperature increase due to the atomic oxygen recombination vs front-face temperature at 200-Pa total air pressure for different ceramic materials.**

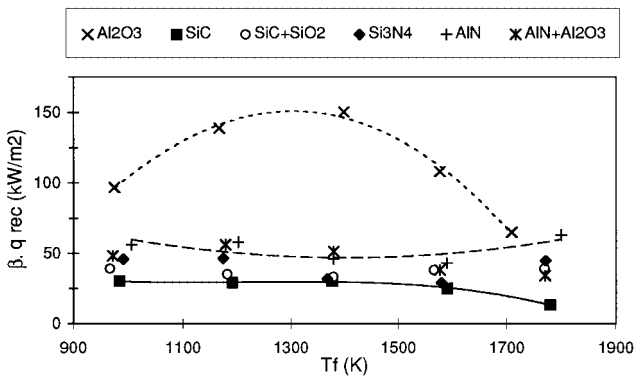


**Fig. 4 Recombination flux transferred to the surface vs front-face temperature for different ceramic materials at a total air pressure of 200 Pa.**

The contribution of the energy due to the microwaves represents about 20–40% of the total temperature increase, and globally the temperature increase due to the catalytic recombination for all of the tested materials decreases rapidly with temperature. The silicon-based ceramics have weaker $\Delta T_f$ than that of the aluminum and particularly of the sintered alumina ($\Delta T_f = 280$ K at 1000 K).

A graphical representation of the results for the recombination fluxes obtained from Eq. (6) is shown in Fig. 4 for some materials tested under 200 Pa at five temperature levels.

The determination of the recombination flux confirms the tendencies obtained with the temperature increase. Silicon-based ceramic materials have similar and low catalytic activities. The sintered SiC has the weakest recombination flux, which is nearly constant between 1000 and 1600 K (around 28 $kW \cdot m^{-2}$), except under active oxidation[21] at 1800 K (13 $kW \cdot m^{-2}$). This confirms its very low catalytic activity; the higher values obtained between 1000 and 1600 K are due to the presence of a thin silica layer formed during the experiment. Aluminum-based ceramic materials have more pronounced catalytic activities, and sintered alumina is by far the more catalytic material, with an increasing recombination flux that reaches 151 $kW \cdot m^{-2}$ at 1400 K before decreasing at 1800 K (66 $kW \cdot m^{-2}$).

#### Bidimensional Model

A bidimensional model has been developed to estimate the radial thermal losses by conduction, which have been neglected in the experimental part. This model is based on the simulation of axial and radial heat transfers in material at high temperature. The bidirectional heat equation is solved with a finite difference scheme, which is applied to a cylindrical shape.[24] The parameters are the sample dimensions, the regular grid, the properties of the materials (density, specific heat, and axial and radial thermal conductivities), and the boundary conditions (emissivity, convective exchange, absorbed solar flux, and temperatures for radiative and conductive heat transfers); recently the microwave heat contribution due to the microwave–material interaction[25–27] has been taken into account, adding a mass flux in the sample.[28]

Injecting the experimental results in the numerical bidimensional model, we establish heat balances for the different plasma environments.

Under air plasma,

$$\alpha \cdot q_{\text{sol}}^{\text{air},*} + q_{\text{mw}}^{\text{air},*} + \beta \cdot q_{\text{rec}}^{\text{air},*} = q_{\text{rad}}^{\text{air},*} + q_{\text{lat}}^{\text{air},*} + q_{\text{conv}}^{\text{air},*} \quad (8)$$

Under argon plasma,

$$\alpha \cdot q_{\text{sol}}^{\text{arg},*} + q_{\text{mw}}^{\text{arg},*} = q_{\text{rad}}^{\text{arg},*} + q_{\text{lat}}^{\text{arg},*} + q_{\text{conv}}^{\text{arg},*} \quad (9)$$

We also suppose $q_{\text{mw}}^{\text{air},*}$ to be equal to $q_{\text{mw}}^{\text{arg},*}$. Therefore, the resolution of the equation system leads to the recombination flux determination. Numerical (two-dimensional) values are given in Tables 1 and 2, respectively, for sintered SiC and $Al_2O_3$. Comparison with the quasi-one-dimensional experimental values shows the same order.

Finally, the studied materials have been classified according to a catalytic scale available between 1000 and 1800 K:

$$SiC \approx SiC + SiO_2 \leq Si_3N_4 \leq AlN \approx AlN + Al_2O_3 \ll Al_2O_3$$

## Chemical Approach: Actinometry

This thermal study is completed with a chemical approach using visible spectroscopy for the determination of the catalytic recombination coefficient. The atomic emission spectroscopy allows the determination of the relative concentration (species/actinometer) to obtain the concentration profile above the sample. This method is limited to low pressure and can be applied with several constraints.

#### Experimental Setup

For the first study, measurements are realized apart from the solar radiation. The samples are tested on the same bench MESOX but without solar exposure. The samples are heated only by microwaves, and so the temperature does not exceed 1000 K.

The spectroscopic bench is composed of an optical sampling system including a lens and an optical fiber and a monochromator equipped with an optical multichannel analyzer (OMA).

The microwave discharge is imaged by the silica lens that focuses the center of the bulk plasma on the entrance face of the optical fiber. The optical emission is sampled parallel to the surface material and transmitted by the optical fiber to the slit entrance of the monochromator. A 60-cm-focal-length monochromator with a 1220-grooves/mm grating is used with a 50-$\mu$m-width slit. The dispersed light is analyzed by means of the 1024 diodes of the OMA detector. Measurements of the atomic spectral lines emitted by the plasma lead to linewidths of the order of 0.07 nm. The small aperture (0.22) of the optical fiber allows spatially resolved measurements. The effective resolution is estimated to be equal to the core diameter (500 $\mu$m) of the used fiber. A micrometric displacement of the sampling system allows analysis of the discharge as a function of the distance to the surface sample.

**Actinometry**

This method is an indirect spectroscopic monitor of the reactive species densities. It has been described elsewhere[29,30] in detail and has been used for the determination of the atomic oxygen density in discharges.[31–34]

A low known quantity of an actinometer (more often argon) is introduced in the flow, and the evolution of the intensities ratio $I_O/I_{Ar}$ of an oxygen line to an argon line is measured along the discharge zone. The constraints of this techniques are as follows:

1) The actinometer must be introduced in low quantity so as not to disturb the plasma.

2) The excited species must be produced by electronic impact from the ground state.

3) The deexcitation of the species must be essentially radiative.

4) The energy dependencies of the cross sections of electronic excitation of O and Ar must be identical in theory, and at the least, the energy thresholds of the transition must be similar.[32]

To determine the spatial variation of the relative concentration of atomic oxygen, we use its most reliable transition at 844.6 nm (Refs. 33 and 34). For the actinometer line, we choose the argon transition at 842.4 nm, which presents an energy threshold (13.1 eV) similar to that for atomic oxygen transition.[32] Thus, it is reasonable to assume that the ratio of the intensities of the two lines is proportional to the oxygen atom concentration. Both of these lines can be recorded simultaneously, thus increasing the accuracy of the intensities ratio measurements.

First, we have studied the influence of the argon percentage introduced in the airflow. Until 8% Ar, the plasma is not modified, and so we choose to work with 7% Ar. Then the influences of microwave-injected power, total pressure, flow rate, and stability of the discharge are studied. By increasing the microwave power, the ratio $I_O/I_{Ar}$ increases very slowly, and so the dissociation of oxygen is nearly constant for power between 300 to 1000 W. The stability of the discharge is measured without the sample, and the ratio $I_O/I_{Ar}$ is constant. Therefore, we have chosen to work at a constant power of 300 W, a total pressure of 200 Pa, and a total flow of $1.11 \times 10^{-6}$ m$^3 \cdot$ s$^{-1}$ with 7% argon.

We consider a cylindrical volume corresponding to the discharge zone, every point being represented by the coordinates $(r, x)$. As the mean free path of the atoms (0.043 cm at 200 Pa) is less than the diameter of the reactor (5 cm), the atom diffusion is given by the diffusion equation written in cylindrical coordinates that describes the variation of the concentration $C_A$ of an atom $A$ vs time for a fixed point in the cylinder $(r, x)$:

$$\frac{\partial C_A}{\partial t} + \mathrm{div} C_A \cdot U_x + \mathrm{div} C_A \cdot U_r + \omega = 0 \qquad (10)$$

where $\omega$ is the variation of the concentration due to the recombination in the gaseous phase and on the reactor walls. We suppose that the convective transfer is negligible because the gas temperature (800 K in these conditions) is near that of the sample.

In steady-state conditions, Eq. (10) becomes

$$D \cdot \left( \frac{\partial^2 C_A}{\partial x^2} + \frac{\partial^2 C_A}{\partial r^2} + \frac{1}{r} \frac{\partial C_A}{\partial r} \right) + \omega = 0 \qquad (11)$$

We also suppose that the radial gradient in the reactor is negligible compared to the axial one, so that the concentration is only a function of $x$. Moreover, the stability of the ratio $I_O/I_{Ar}$ in the reactor allows neglecting the recombination in volume and on the reactor wall.

Thus, Eq. (11) can be simplified to

$$D \cdot \frac{\partial^2 C_A}{\partial x^2} = 0 \qquad (12)$$

This equation has two limit conditions.

1) The ratio $I_O/I_{Ar}$ is constant along the discharge; thus, far from the sample, the concentration has a known fixed value:

$$C(x = 0) = C_0 = \text{const} \qquad (13)$$

2) At the surface sample $(x = L)$, the mass balance in oxygen atoms is established by the equality between the oxygen arriving at the surface by diffusion and the atomic oxygen recombined at the surface:

$$-D_{O,air} \cdot \left. \frac{\partial C_O}{\partial x} \right|_{x=L} - C_O(x = L) \cdot \frac{\gamma \cdot V^*}{4} = 0 \qquad (14)$$

with $V^*$ the mean square velocity of oxygen atoms written as

$$V^* \approx \sqrt{\frac{N_A \cdot k_B \cdot Tg}{M_O}} \qquad (15)$$

The evolution of the atomic oxygen concentration is given by the solution of Eq. (12).

As with the actinometry method, the ratio of the concentration is proportional to the intensity ratio of the emitted lines. Thus, because argon is an inert gas with constant concentration along axis $x$, we deduce

$$\frac{C_0}{C(x = L)} = \frac{(I_O/I_{Ar})_{x=0}}{(I_O/I_{Ar})_{x=L}} = \frac{R_0}{R_L} \qquad (16)$$

with $R_0$ and $R_L$ the ratio of the intensities $I_O/I_{Ar}$, respectively, at the entrance of the reactor $(x = 0)$ and at the surface sample $(x = L)$.

Finally, the intensities ratio obtained by actinometry leads to the determination of the recombination coefficient $\gamma$ by the following equation:

$$\gamma = \left( \frac{R_0}{R_L} - 1 \right) \cdot \frac{4 \cdot D_{O,air}}{V^* \cdot L} \qquad (17)$$

We have applied this method on sintered SiC, oxidized SiC (sintered SiC + $SiO_2$), and sintered alumina. The intensities ratio $I_O/I_{Ar}$ functions of the distance to the surface sample are shown in Fig. 5 for the case of sintered $Al_2O_3$.

The uncertainties $\Delta\gamma/\gamma$ have been calculated taking into account the errors in $R_0$, $R_L$ (10%), and $L$ (7%), as well as in the flow parameters: the diffusion coefficient determined using Chapman–Enskog theory, $D_{O,air} = 695$ cm$^2$/s, and the mean square atomic velocity determined using the gas kinetic theory (rarefied gas), $V^* = 645$ m/s; the accuracy of these values is due essentially to that of the gas temperature (20%) (measured by emission spectroscopy), leading to a total accuracy of 65%.

In all cases, we observe a constant level for the concentration profile until 6 mm from the surface led by a progressive decrease, and then, at 2 mm from the surface, there is a change in the slope that we consider representative of the catalytic phenomena occurring on the material surface.

The values of the recombination coefficient have been calculated for each material with the concentration profile. The obtained values are

$$\gamma_O(\mathrm{SiC}) = 0.008 \pm 65\% \quad \text{for} \quad T = 870\,\mathrm{K}$$

$$\gamma_O(\mathrm{SiO_2}) = 0.010 \pm 65\% \quad \text{for} \quad T = 850\,\mathrm{K}$$

$$\gamma_O(\mathrm{Al_2O_3}) = 0.085 \pm 65\% \quad \text{for} \quad T = 940\,\mathrm{K}$$

These results show the very weak catalytic activity of SiC and silica, the latter being slightly more catalytic at this temperature. The recombination coefficient of alumina, however, is higher by one order of magnitude than that of SiC, justifying greater catalytic activity.

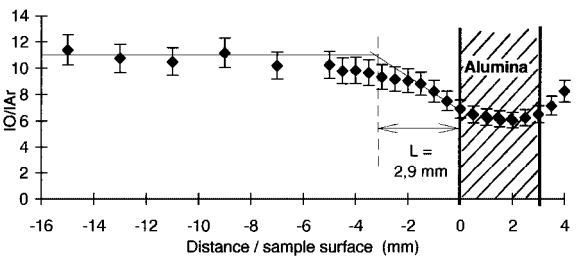


**Fig. 5 Relative atomic oxygen concentration profile $I_O/I_{Ar}$ in the discharge vs distance above a sample of sintered $Al_2O_3$ at 200-Pa total air pressure.**

We can observe that the alumina temperature (heated only by microwaves) is higher than those of silicon-based material because, as we have seen in the thermal study, the interaction between microwave and material is higher for alumina. We have to take into account this temperature difference (nearly 80 K), but this cannot justify the catalycity difference.

Comparison with literature data is difficult because most of the studies are realized at room temperatures (or at higher temperature, more than 1400 K) and on different chemical surfaces, but our experimental results seem to have a correct order of magnitude if we use the results on silica of Jumper and Seward[2] ($\gamma = 1.4 \times 10^{-2}$ at 900 K) and Greaves and Linnett[35] ($\gamma = 10^{-2}$ at 893 K). Kim and Boudart[11] find lower values ($\gamma = 2 \times 10^{-4}$ at 920 K). The reaction-cured glass coating (borosilicate glass) gives different values according to Rakich et al.[36] ($\gamma = 5 \times 10^{-4}$) or Stewart et al.[5] ($\gamma = 10^{-3}$). The results obtained by the Deutschmann et al.[14] and Nasuti et al.[15] modelizations agree with our value, both giving $\gamma = 10^{-2}$ at 900 K, but the Daiss et al.[20] result is lower by one order of magnitude.

## Concluding Remarks

The determination of the atomic oxygen recombination at the surface of different sintered ceramic materials at high temperature under low-air-pressure plasma has been realized in the MESOX setup using thermal and chemical approaches.

The thermal method is based on the study of the thermal behavior of materials under air and argon plasmas (microwave-excited gas, sample in the discharge), with a roughly Lambertian surface. This approach leads to the determination of the temperature increase due to the catalytic recombination of atomic oxygen and to the evaluation of the recombination flux transferred at the surface. A low influence of the pressure has been observed between 200- and 2000-Pa air, which can come from a limitation of the recombination by the number of active sites and the prevalence of the Eley–Rideal mechanism, with recombination reactions between an atom in the gaseous phase and one adsorbed, this being in accordance with literature results. The temperature increase is more pronounced at low temperature levels and decreases rapidly with suface temperature. Catalytic recombination fluxes have also been calculated from the heat balance with a one-dimensional hypothesis. Catalytic activities for the different materials move weakly between 1000 and 1400 K, except for $Al_2O_3$ for which recombination fluxes vary strongly and reach a maximum at 1400 K. Most of the studied materials are weakly catalytic (except $Al_2O_3$) and are classified according to a catalytic scale available between 1000 and 1800 K: $SiC \approx SiC + SiO_2 \leq Si_3N_4 \leq AlN \approx AlN + Al_2O_3 \ll Al_2O_3$.

The chemical approach using actinometry by emission spectroscopic measurements have given good first results at around 1000 K, for the three materials tested, and partially confirms the experimental thermal results. This chemical evaluation is actually transferred at high temperature simultaneously with the thermal method to obtain both the recombination flux and the recombination coefficient $\gamma$ in the same range of temperature (1000–1800 K) but only at 200 Pa due to the validity of actinometry measurements.

## Acknowledgment

The authors wish to thank the European Space Agency for support of this work.

## References

[1]Scott, C. D., "Catalytic Recombination of Nitrogen and Oxygen on High-Temperature Reusable Surface Insulation," AIAA Paper 80-1477, July 1980.

[2]Jumper, E. J., and Seward, W. A., "Model for Oxygen Recombination on Reaction-Cured Glass," *Journal of Thermophysics and Heat Transfer*, Vol. 8, No. 3, 1994, pp. 460–465.

[3]Kolodzeij, P., and Stewart, D. A., "Nitrogen Recombination on High-Temperature Reusable Surface Insulation and the Analysis of Its Effect on Surface Catalysis," AIAA Paper 87-1637, June 1987.

[4]Willey, R. J., "Comparison of Kinetics Models for Atoms Recombination on High-Temperature Reusable Surface Insulation," *Journal of Thermophysics and Heat Transfer*, Vol. 7, No. 1, 1993, pp. 55–62.

[5]Stewart, D. A., Rakich, J. V., and Lanfranco, M. J., "Catalytic Surface Effects on Space Shuttle Thermal Protection System During Earth Entry of Flights STS-2 Through STS-5," NASA CP-2283, Pt. 2, March 1983, pp. 827–845.

[6]Zoby, E. V., Gupta, R. N., and Simmonds, A. L., "Temperature Dependent Reaction Rate Expressions for Oxygen Recombination," *Thermal Design of Aeroassisted Orbital Transfer Vehicles*, edited by H. P. Nelson, Vol. 96, Progress in Astronautics and Aeronautics, AIAA, Washington, DC, 1985, pp. 445–464.

[7]Clark, R. K., Cunnington, G. R., and Wiedemann, K. E., "Determination of the Recombination Efficiency of Thermal Control Coatings for Hypersonic Vehicles," *Journal of Spacecrafts and Rockets*, Vol. 32, No. 1, 1995, pp. 89–96.

[8]Cunnington, G., Robinson, J., and Clark, R., "Noncatalytic Coatings for Hypersonic Vehicle Applications," AIAA Paper 90-1742, June 1990.

[9]Vasil'evskii, S. A., Kolesnikov, A. F., and Yakushin, M. I., "Determination of the Effective Probabilities of the Heterogeneous Recombination of Atoms when Heat Flow Is Influenced by Gas-Phase Reactions," *High Temperature*, Nov. 1991, pp. 411–418.

[10]Gordeev, A. N., Kolesnikov, A. F., and Yakushin, M. I., "An Induction Plasma Application to Buran's Heat Protection Tile Ground Tests," *SAMPE Journal*, Vol. 28, No. 3, 1992, pp. 29–33.

[11]Kim, Y. C., and Boudart, M., "Recombination of O, N and H Atoms on Silica: Kinetics and Mechanism," *Langmuir*, Vol. 7, 1991, pp. 2999–3005.

[12]Pallix, J. B., and Copeland, R. A., "Measurement of Catalytic Recombination Coefficients on Quartz Using Laser-Induced Fluorescence," *Journal of Thermophysics and Heat Transfer*, Vol. 10, No. 2, 1996, pp. 224–233.

[13]N'Guyen-Xuan, F., Hassouni, K., Cavvadias, S., and Amouroux, J., "Measurement of the Oxygen Recombination Coefficient on Poorly Catalytic Surfaces by Actinometry Using OMA Detection," *Proceedings of the 11th International Symposium on Plasma Chemistry* (Loughborough, England, UK), Vol. 4, 1993, pp. 1516–1521.

[14]Deutschmann, D., Riedel, U., and Warnatz, J., "Modeling of Nitrogen and Oxygen Recombination on Partial Catalytic Surfaces," *Journal of Heat Transfer*, Vol. 117, 1995, pp. 495–501.

[15]Nasuti, F., Barbato, M., and Bruno, C., "Material-Dependent Catalytic Recombination Modeling for Hypersonic Flows," *Journal of Thermophysics and Heat Transfer*, Vol. 10, No. 1, 1996, pp. 131–136.

[16]Halpern, B., and Rosner, D. E., "Chemical Energy Accommodation at Catalyst Surfaces," *Transactions of the Faraday Society*, Vol. 74, No. 8, 1978, pp. 1883–1912.

[17]Melin, G. A., and Madix, R. J., "Energy Accommodation During Oxygen Atom Recombination on Metal Surfaces," *Transactions of the Faraday Society*, Vol. 67, 1971, pp. 198–211.

[18]Carleton, K. L., and Marinelli, W. J., "Spacecraft Thermal Energy Accommodation from Atomic Recombination," *Journal of Thermophysics and Heat Transfer*, Vol. 6, No. 4, 1992, pp. 650–655.

[19]Clark, R. K., Cunnington, G. R., and Robinson, J. C., "Vapor-Deposited Emittance-Catalysis Coatings for Superalloys in Heat Shield Applications," *Journal of Thermophysics*, Vol. 1, No. 1, 1987, pp. 28–34.

[20]Daiss, A., Frühauf, H. H., and Messerschmid, E. W., "Modeling of Catalytic Reactions on Silica Surfaces with Consideration of Slip Effects," AIAA Paper 96-1903, June 1996.

[21]Balat, M. J. H., "Determination of the Active-to-Passive Transition in the Oxidation of Silicon Carbide in Standard and Microwave-Excited Air," *Journal of European Ceramic Society*, Vol. 16, 1996, pp. 55–62.

[22]Balat, M., Czerniak, M., and Olalde, G., "Catalycity at High Temperature: New Approach for Evaluation," *High Temperature Chemical Processes*, Vol. 3, 1994, pp. 325–334.

[23]Czerniak, M., "Oxydation et Recombinaison Catalytique à la Surface de Matériaux Céramiques soumis à des Conditions de Rentré atmosphérique terrestre (Haute Température, Plasma d'Air basse Pression)," Ph.D. Thesis, Univ. Bordeaux I, Bordeaux, France, Feb. 1996.

[24]Ferrière, A., and Philippot, E., "Méthode de Résolution par Différences finies de l'Équation de la Chaleur en Géométrie bidirectionnelle cylindrique anisotrope," Internal Rept., Inst. de Science et de Génie des Matériaux et Procédés, Centre National de la Recherche Scientifique, Font-Romeu, France, Feb. 1994.

[25]Tinga, W. R., "Fundamental of Microwave-Material Interactions and Sintering," Vol. 124, *Microwave Processing of Materials*, edited by W. H. Sutton, *Materials Research Society Symposium Proceedings*, 1988, pp. 33–43.

[26]Kenkre, V. M., "Theory of Microwave Interactions with Ceramic Materials," *Ceramic Transactions*, Vol. 21, 1991, pp. 69–80.

[27]Spotz, M. S., Skamser, D. J., and Johnson, D. L., "Thermal Stability of Ceramic Materials in Microwave Heating," *Journal of American Ceramic Society*, Vol. 78, No. 4, 1995, pp. 1041–1048.

[28]Restoux, J. R., "Modélisation du Flux de Recombianaison catalytique de l'Oxygène atomique à haute Température—Apport énergétique de l'Interaction Microonde-Matériau," Student Lab. Rept., Inst. de Science et de Génie des Matériaux et Procédés, Centre National de la Recherche Scientifique, Font-Romeu, France.

[29]Coburn, J. W., and Chen, M., "Optical Emission Spectroscopy of Reactive Plasmas: A Method for Correlating Emission Intensities to Reactive Particle Density," *Journal of Applied Physics*, Vol. 51, No. 6, 1980, pp. 3134–3136.

[30]Kiss, L. D. B., Nicolai, J. P., Conner, W. T., and Sawin, H. H., "CF and $CF_2$ Actinometry in $CF_4$/Ar plasma," *Journal of Applied Physics*, Vol. 71, No. 7, 1992, pp. 3186–3192.

[31]Diamy, A. M., Legrand, J. C., Al Andari, J., and Ben-Aïm, R. L., "Atomic Oxygen Titration in the Discharge and in the Post-Discharge of Oxygen MIP," *9th Symposium on Plasma Chemistry* (Pugnochiuso, Italy), ISCP 9, edited by R. d'Agostino, Vol. 1, 1989, pp. 591–596.

[32]Booth, J. P., Joubert, O., Pelletier, J., and Sadeghi, N., "Oxygen Atom Actinometry Reinvestigated: Comparison with Absolute Measurements by Resonance Absorption at 130 nm," *Journal of Applied Physics*, Vol. 69, No. 2, 1991, pp. 618–626.

[33]Granier, A., Chéreau, D., Henda, K., Safari, R., and Leprince, P., "Validity of Actinometry to Monitor Oxygen Atom Concentration in Microwave Discharges Created by Surface Wave in $O_2$–$N_2$ Mixtures," *Journal of Applied Physics*, Vol. 75, No. 1, 1994, pp. 104–114.

[34]Pagnon, D., Amorim, J., Nahorny, J., Touzeau, M., and Vialle, M., "On the Use of Actinometry to Measure the Dissociation in $O_2$ DC Glow Discharges: Determination of the Wall Recombination Probability," *Journal of Physics D: Applied Physics*, Vol. 28, 1995, pp. 1856–1868.

[35]Greaves, J. C., and Linnett, J. W., "Recombination of Atoms at Surfaces—Part 6—Recombination of Oxygen Atoms on Silica from 20°C to 600°C," *Transactions of the Faraday Society*, Vol. 55, 1959, pp. 1346–1354.

[36]Rakich, J. V., Stewart, D. A., and Lanfranco, M. J., "Results of a Flight Experiment on the Catalytic Efficiency of the Space Shuttle Heat Shield," AIAA Paper 82-0944, June 1982.

B. A. Bhutta
*Associate Editor*